The Kv2.2 channel mediates the inhibition of Prostaglandin E2 on glucose-stimulated insulin secretion in pancreatic β-cells

Chengfang Pan[1,2]†, Ying Liu[3]†, Liangya Wang[1,2], Wengyong Fan[1], Yunzhi Ni[3], Xuefeng Zhang[1], Di Wu[3], Chenyang Li[1], Jin Li[1], Zhaoyang Li[4*], Rui Liu[3*], Changlong Hu[1,2*]

1. School of Life Sciences, Fudan University, Shanghai, 200438, China.
2. International Human Phenome Institute (Shanghai), Shanghai, 200433, China.
3. Department of Endocrinology and Metabolism, Huashan Hospital, Fudan University, Shanghai, 200040, China.
4. State Key Laboratory of Medical Neurobiology and MOE Frontiers Center for Brain Science, and the Institutes of Brain Science, Fudan University, Shanghai, 200032, China.

†, These authors contribute equally to the work.

***Corresponding authors:** Changlong Hu (clhu@fudan.edu.cn); ZhaoyangLi (lzy@fudan.edu.cn); Rui Liu (fd_ruiliu@fudan.edu.cn),

Abstract

Prostaglandin E2 (PGE2) is an endogenous inhibitor of glucose-stimulated insulin secretion (GSIS) and plays an important role in pancreatic β-cell dysfunction in type 2 diabetes mellitus (T2DM). This study aimed to explore the underlying mechanism by which PGE2 inhibits GSIS. Our results showed that PGE2 inhibited Kv2.2 channels via increasing PKA activity in HEK293T cells overexpressed with Kv2.2 channels. Point mutation analysis demonstrated that S448 residue was responsible for the PKA-dependent modulation of Kv2.2. Furthermore, the inhibitory effect of PGE2 on Kv2.2 was blocked by EP2/4 receptor antagonists, while mimicked by EP2/4 receptor agonists. The immune fluorescence results showed that EP1-EP4 receptors are expressed in both mouse and human β-cells. In INS-1(832/13) β-cells, PGE2 inhibited voltage-gated potassium currents and electrical activity through EP2/4 receptors and Kv2.2 channels. Knockdown of Kv2.2 reduced the action potential firing frequency and alleviated the inhibition of PGE2 on GSIS in INS-1(832/13) β-cells. PGE2 impaired glucose tolerance in wild-type mice but did not alter glucose tolerance in Kv2.2 knockout mice. Knockout of Kv2.2 reduced electrical activity, GSIS and abrogated the inhibition of PGE2 on GSIS in mouse islets. In conclusion, we have demonstrated that PGE2 inhibits GSIS in pancreatic β-cells through the EP2/4-Kv2.2 signaling pathway. The findings highlight the significant role of Kv2.2 channels in the regulation of β-cell repetitive firing and insulin secretion, and contribute to the understanding of the molecular basis of β-cell dysfunction in diabetes.

Introduction

Prostaglandin E2 (PGE2) is the major prostaglandin formed in pancreatic islets and is closely related to islet β-cell dysfunction (Meng et al., 2006; Oshima, Taketo, & Oshima, 2006; Vennemann et al., 2012). As an endogenous inhibitor of glucose-stimulated insulin secretion (GSIS), PGE2 plays an important role in type 2 diabetes mellitus (T2DM) (Carboneau, Breyer, & Gannon, 2017). PGE2 has been demonstrated to inhibit GSIS in both mouse models of T2DM and in pancreatic islets obtained from human organ donors with T2DM (Kimple et al., 2013; Neuman et al., 2017; Parazzoli et al., 2012). Recent studies have shown that plasma levels of PGE2 are correlated with T2DM status, and it has the potential to be a marker of T2DM status (Fenske et al., 2022; Truchan et al., 2021). However, the underlying mechanism for the PGE2 inhibition of GSIS is not fully understood.

PGE2 functions through the activation of four specific G-protein-coupled receptor subtypes, termed EP1-4. The EP1 receptor couples to G_q and causes an intracellular Ca^{2+} increase. The EP2 and EP4 receptors couple to G_s to increase intracellular cAMP formation, while the EP3 receptor couples to G_i to decrease intracellular cAMP production (Sugimoto & Narumiya, 2007). The mRNA expression of all four EP receptors is found in rat, mouse, and human pancreatic islets (Bramswig et al., 2013; Tran, Gleason, & Robertson, 2002; Vennemann et al., 2012). Among all EP receptors, the EP3 receptor has attracted widespread attention due to its high expression on β-cells in diabetic mouse models (elevated more than 40 times compared to non-diabetic mice)(Kimple et al., 2013). Currently, it is considered the primary effector for PGE2 in GSIS. Islets from diabetic BTBR mice exhibit increased GSIS when treated with the EP3 antagonist L-798106, and show decreased GSIS after treated with the EP3 agonist PGE1 (Shridas, Zahoor, Forrest, Layne, & Webb, 2014). However, increasing evidence suggests that EP3 plays a role only in insulin secretion under T2DM (Carboneau et al., 2017). In human islets from non-diabetic donors, the EP3 antagonist L-798106 does not affect GSIS, but improves insulin secretion in islets from donors with T2DM (Kimple et al., 2013). Ceddia et al. reported that the EP3 antagonist DG-041 does not affect GSIS in islets from non-diabetic human or wild-type mice on a chow diet, and that global gene knockout of EP3 in mice does not alter GSIS (Ceddia et al., 2016).The impact of the PGE2 signaling pathway on nondiabetic β-cell function remains unclear. Moreover, the roles of EP1, EP2,

and EP4 receptors in GSIS are rarely reported.

Pancreatic β-cells are electrical excitable. GSIS is associated with a complex electrical activity, which is regulated by various voltage-gated plasmalemmal ion channels (Braun et al., 2008; S. N. Yang et al., 2014). The Kv2 channel family, which consists of Kv2.1 and Kv2.2, plays a crucial role in modulating neural excitability (Liu & Bean, 2014). The effect of Kv2.1 channels on insulin secretion has been well studied. In rodents, Kv2.1 is recognized as the primary facilitator of delayed rectifier potassium currents in β-cells. Suppressing Kv2.1 results in heightened glucose-stimulated membrane potential amplitude, consequently enhancing GSIS in mouse pancreatic β-cells (Jacobson et al., 2007; MacDonald et al., 2002). However, Kv2.1 inhibitor stromatoxin shows little effect on human β-cell electrical function or insulin secretion (Braun et al., 2008), despite the presence of Kv2.1 protein in human islets (Tamarina, Kuznetsov, Fridlyand, & Philipson, 2005). Increasing evidence suggests that Kv2.1 regulates insulin secretion through channel clusters independently of its electrical function (Dai et al., 2012; Fu et al., 2017; Greitzer-Antes et al., 2018). Recent studies have shown that human islet β-cells express both Kv2.1 and Kv2.2 channels, with much higher levels of Kv2.2 mRNA expression (Blodgett et al., 2015; Fu et al., 2017). Jensen et al. reported that Kv2.2 expression is also involved in GSIS (Jensen et al., 2013). Nevertheless, the functions of the Kv2.2 channel in the *in vivo* physiology of islet β-cells have not been definitively established.

In this study, we investigated the role of EP1-4 receptors and Kv2.2 in the inhibitory effect of PGE2 on insulin secretion in pancreatic β-cells and Kv2.2 knockout mice. Our findings indicate that: 1) PGE2 reduces Kv2.2 currents via the EP2/4-PKA signaling pathway; 2) PGE2 inhibits β-cell electrical activity through Kv2.2 channels; 3) Knockout of Kv2.2 channels abrogates the PGE2 induced inhibition of GSIS. These results suggest that EP2/4 receptors and Kv2.2 channels play crucial regulatory roles in the normal physiological secretion of insulin.

Results

PGE2 inhibits Kv2.2 currents via the EP2/EP4 signaling pathway in HEK293T cells.

We initially conducted experiments to assess the impact of PGE2 on Kv2.2 channels. Kv2.2

channels were overexpressed in HEK293T cells, and Kv2.2 currents were elicited by a 200-ms depolarization pulse from -80 to +40 mV. Extracellular application of 10 μM PGE2 significantly inhibited Kv2.2 currents. This inhibition was rapid, reaching its maximum effect in approximately 6 minutes (Fig. 1A and B). The inhibitory effect of PGE2 on Kv2.2 is dose-dependent, with the maximum effect at around 10 μM (Fig. 1C). Therefore, we used 10 μM PGE2 for the subsequent experiments. The I-V curve demonstrated that PGE2 significantly inhibited Kv2.2 currents at all positive testing potentials above +20 mV (Fig. 1D). Moreover, 10 μM PGE2 did not alter the steady-state activation and inactivation properties of Kv2.2 currents (Fig. 1E and F).

Next, we investigated the mechanism of PGE2 inhibition on Kv2.2 channels. PGE2 functions by activating EP1-4 receptors. We investigated the mRNA and protein expression profiles of EP receptors in HEK293T cells. The mRNAs for all four EP receptors were detected in HEK293T cells, with notably higher levels observed for EP2 and EP4 (Fig. 2A). Furthermore, immunofluorescence results confirmed the presence of protein expression for EP1-EP4 receptors in HEK293T cells (Fig. 2B). To determine which EP receptor is responsible for the PGE2-induced inhibition, we applied SC51089 (10 μM, the EP1 receptor antagonist) (Zhou, Qian, Chou, & Iadecola, 2008), AH6809 (20 μM, the EP2 receptor antagonist) (Srinivasalu et al., 2020), L798106 (10 μM, the EP3 receptor antagonist) (Corboz et al., 2021), and AH23848 (20 μM, the EP4 receptor antagonist)(He et al., 2021) to the extracellular solution to selectively inhibit the respective EP receptors. The acute application of the four antagonists alone had no effect on Kv2.2 currents (Fig. 2C). Pretreatment with SC51089 and L798106 for 10 min did not alter the PGE2-induced inhibition. However, pretreatment with AH6809 and AH23848 partially blocked the PGE2-induced inhibition (Fig. 2D and E). Furthermore, the EP2 receptor agonist Butaprost (20 μM) and the EP4 receptor agonist CAY10598 (20 μM) both inhibited Kv2.2 currents (Fig. 2F and G). These results suggest that PGE2 inhibits Kv2.2 via EP2/EP4 signaling pathway.

PGE2 inhibits Kv2.2 currents via the PKA signaling pathway in HEK293T cells.

The EP2 and EP4 receptors couple to Gs, increasing intracellular cAMP formation and activating the PKA signaling pathway (Sugimoto & Narumiya, 2007). We investigated

whether PGE2 regulates Kv2.2 via PKA. Treatment with 10 μM PGE2 rapidly increased PKA activity in HEK293T cells (Fig. 3A). The PKA activator, Db-cAMP, could mimic the inhibitory effect of PGE2 on Kv2.2 channels (Fig. 3B). The PKA inhibitor, Rp-cAMP, had no effect on Kv2.2 currents (Fig. 3C). However, pre-incubation with Rp-cAMP blocked the inhibitory effect of PGE2 on Kv2.2 channels in HEK293T cells (Fig. 3D). These findings illustrate that PGE2 inhibits Kv2.2 currents through the PKA signaling pathway.

We further investigated whether PKA regulates Kv2.2 currents via direct phosphorylation of the channel. The Kv2.2 channel protein contains approximately nine putative phosphorylation sites that conform to the minimal consensus sequence for PKA, according to https://scansite4.mit.edu. The positions of the nine sites are depicted in Figure 3E. To identify the specific site responsible for PKA regulation of Kv2.2 channels, we introduced mutations in the amino acid sequence. We replaced all nine amino acids with aspartic acid to mimic the PKA phosphorylation state of Kv2.2 channels. Among the nine mutations, only the S448D mutation yielded a significant reduction in Kv2.2 currents (Fig. 3F). Notably, the S448D mutation also abrogated the inhibitory effect of PGE2 on Kv2.2 (Fig. 3G). To further confirm the role of the S448 site in PGE2-induced inhibition of Kv2.2, we also conducted a mutation, changing S448 to alanine (S448A). This mutation effectively prevented the inhibitory effect of PGE2 on Kv2.2 currents (Fig. 3H). These data indicate that the S448 site is responsible for the PGE2-induced inhibition of Kv2.2 currents.

PGE2 inhibits endogenous Kv2.2 currents through the EP2/EP4 signaling pathway in INS-1(832/13) β-cells.

To investigate the physiological function of PGE2-induced inhibition of Kv2.2, we examined whether PGE2 could also affect the native Kv2.2 currents in pancreatic β-cells. Previous study has demonstrated that Kv2.2 channels contribute to the delayed rectifier outward K^+ currents in pancreatic β-cells (Fu et al., 2017). Consistent with these studies, we observed the protein expression of Kv2.2 channels in INS-1(832/13) β-cells (Fig. 4A). The voltage-dependent potassium currents (I_K) in INS-1(832/13) cells were elicited by a 200-ms depolarization pulse from -80 to +40 mV, and the extracellular application of 10 μM PGE2 significantly inhibited the I_K (Fig. 4B).

To assess the contribution of Kv2.2 channels to the PGE2-induced inhibition in INS-1(832/13) cells, we knocked down the expression of Kv2.2 using shRNA. The efficiency of the two shRNAs, named KD1-Kv2.2 and KD2-Kv2.2, were first evaluated in HEK293T cells overexpressing Kv2.2. KD2-Kv2.2 showed higher efficiency than KD1-Kv2.2 and was selected for subsequent experiments (Fig. 4C). Knockdown of Kv2.2 by KD2-Kv2.2 significantly reduced endogenous K^+ currents (Fig. 4D) in INS-1(832/13) cells, and abrogated PGE2-induced inhibition of K^+ currents (Fig. 4E and F). Furthermore, the EP2 receptor agonist Butaprost (20 μM) and the EP4 receptor agonist CAY10598 (20 μM) both inhibited the I_K in INS-1(832/13) cells (Fig. 4G and H), confirming that it is the same signaling pathway as that in HEK293T cells.

PGE2 reduces electrical activity via Kv2.2 channels in INS-1(832/13) cells.

GSIS is associated with β-cell electrical activity, which is regulated by Kv2 potassium channels (Drews, Krippeit-Drews, & Dufer, 2010). Therefore, we tested whether PGE2 affects β-cell electrical activity. We found that 10 μM PGE2 reduced action potential (AP) frequency and increased AP half-width in INS-1(832/13) cells with little effect on the peak amplitude of AP (Fig. 5A and B). Furthermore, knockdown of Kv2.2 with Kv2.2-specific shRNA abrogated PGE2-induced effect on INS-1(832/13) cells (Fig. 5C). This suggests that PGE2 reduces electrical activity via Kv2.2 channels in INS-1(832/13) cells. Since PGE2 inhibits Kv2.2 via EP2/4 receptors, it is plausible to hypothesize that PGE2 reduces electrical activity via EP2/4 receptors in INS-1(832/13) cells. To test the hypothesis, we first investigated the expression of EP receptors in INS-1(832/13) cells. Immunofluorescence results revealed that all EP1-EP4 receptors are expressed in INS-1(832/13) cells (Fig. 5D). In addition, both mouse and human islet β-cells were found to express all four EP receptors (Fig. 5E). As expected, the EP2 receptor agonist Butaprost (20 μM) and the EP4 receptor agonist CAY10598 (20 μM) both inhibited AP frequency in INS-1(832/13) cells (Fig. 6A and B). This indicates that PGE2 reduces electrical activity via EP2/4 in INS-1(832/13) cells.

PGE2 regulates insulin secretion through Kv2.2 channels in INS-1(832/13) cells and mice.

We next investigated whether Kv2.2 regulates the effect of PGE2 on GSIS in INS-1(832/13)

cells. As expected, 10 μM PGE2 significantly reduced GSIS with little effect on basal insulin secretion in INS-1(832/13) cells (Fig. 7A). Knockdown of Kv2.2 with KD2 shRNA did not alter basal insulin secretion but reduced GSIS in INS-1(832/13) cells (Fig. 7B). Moreover, knockdown of Kv2.2 with KD2 shRNA greatly alleviated the inhibitory effect of PGE2 on GSIS (percent inhibition: scramble, 62%; KD2, 14%, Fig.7B).

To investigate the physiological role of Kv2.2 during GSIS *in vivo*, a mouse model was utilized in which the Kv2.2 coding gene is disrupted at exon 2 (Fig. 7C). The targeting cassette removes 446 bp in exon 2 of the Kv2.2 coding gene sequence. The disrupted sequence is detected using PCR to produce one amplicon with one primer inside the targeting sequence in combination with one Kv2.2 specific primer outside the targeting sequence (Fig. 7C). The Kv2.2 protein was detected only in wild-type islets using a Kv2.2-specific antibody (Fig. 7D). The body weight of the Kv2.2 knockout mice was similar to that of the wild-type littermates (Fig. 7E). Kv2.2$^{-/-}$ mice were assessed for possible impairment in glucose homeostasis using an intraperitoneal glucose tolerance test. Kv2.2$^{-/-}$ mice had similar fasting blood glucose levels with control group (Fig. 7F). PGE2 treatment worsened glucose tolerance in control animals but had little effect on Kv2.2$^{-/-}$ mice (Fig. 7F). This suggests that PGE2 modulates GSIS *in vivo* through Kv2.2 channels. The Kv2.2 gene knockout mice used in this study are global knockouts. To further confirm the role of Kv2.2 in insulin secretion, we isolated pancreatic islets for GSIS experiments. Islets from Kv2.2$^{-/-}$ mice exhibited reduced GSIS compared to islets from wild-type mice (Fig. 7G). While PGE2 reduced GSIS in islets from wild-type mice, it had little effect on GSIS in islets from Kv2.2$^{-/-}$ mice (Fig. 7G).

PGE2 reduces electrical activity via Kv2.2 channels in mouse β-cells within islets.

Finally, we investigated the effect of PGE2 on the electrical activity of β-cells within islets. The I_K in Kv2.2$^{-/-}$ β-cells showed significantly reduced amplitudes (Fig. 8A). Similar to our observations in INS-1(832/13) cells above, 10 μM PGE2 inhibited I_K in mouse β-cells, and Kv2.2 ablation abolished the inhibitory effect of PGE2 (Fig. 8B). PGE2 reduced the firing frequency of AP induced by 20 mM glucose in β-cells within islets, while had little effect on the AP peak amplitude and half-width (Fig. 8C). Furthermore, the effect of PGE2 on mouse

islet β -cell electrical activity was abrogated by knockout of Kv2.2 (Fig. 8D).

Discussion

While EP3 has been demonstrated to exert an inhibitory influence on GSIS, increasing evidence suggests that the impact of EP3 may manifest primarily when β-cell dysfunction is already established, as observed in T2DM (Carboneau et al., 2017; Truchan et al., 2021). In our current investigation, we unveil that Kv2.2 channels play a crucial role in regulating β-cell repetitive firing and insulin secretion. PGE2 inhibits Kv2.2 channels via the EP2/4 signaling pathway, consequently impeding GSIS in normal β-cells.

Even though the previous study reported that the EP2 protein-encoding gene *Ptger2* was not identified by RNA-seq in mouse islets (Ku et al., 2012). Other studies have shown that the mRNA expression of all four EPs is observed in rat, mouse, and human pancreatic islets (Bramswig et al., 2013; Tran et al., 2002; Vennemann et al., 2012). In our current study, we provide evidence demonstrating the presence of protein expression for all four types of PGE2 receptors in both human and mouse pancreatic β-cells. In comparison to EP3, our knowledge of the impact of EP1, EP2, and EP4 on insulin secretion is currently limited. Tran et al. have reported that the EP1 antagonist fails to impede the inhibitory effects of IL-1β on GSIS in isolated rat islets. EP3 agonists, such as misoprostol or sulprostone, decrease GSIS through Gi proteins in rat islets (Tran et al., 2002). A recent study has unveiled that the activation of Gi/o protein-coupled receptors leads to the stimulation of Na^+/K^+ ATPase. This stimulation, in turn, hyperpolarizes the membrane potential of β-cells, consequently suppressing β-cell electrical excitability and insulin secretion (Dickerson et al., 2022). Consequently, one would anticipate that PGE2 activates Gi protein-coupled EP3 receptors, thereby inhibiting insulin secretion through membrane potential hyperpolarization and the reduction of β-cell electrical excitability. Surprisingly, no alterations in β-cell membrane potential were observed following PGE2 treatments. We found that PGE2 inhibits Kv2.2 channels and electroactivity of β-cells via G_s- coupled EP2/4 receptors instead of EP3 receptors. PGE2 is likely to predominantly exert its effects via the EP2/4 receptors in normal β-cells. However, in instances of established β-cell dysfunction, such as in T2DM, it appears that PGE2 may act through the upregulated EP3 receptors (Kimple et al., 2013). This study found that activating

either EP2 or EP4 receptors can inhibit Kv2.2 channels, and further research is needed to determine which receptor is the primary regulatory factor for GSIS.

Both Kv2.1 and Kv2.2 contribute to the delayed outward K^+ current in human β-cells, and their mRNA expression in diabetic islets is lower than that in non-diabetic islets (Fu et al., 2017). Kv2.1 channels in cell membrane exist in two forms: clustered and non-clustered. Non-clustered Kv2.1 channels conduct K^+ normally, while clustered Kv2.1 channels are barely conductive (Fox, Loftus, & Tamkun, 2013). A recent study has shown that Kv2.1 channels form clusters in INS-1(832/13) cells and human β-cells (Fu et al., 2017). Kv2.1-mediated insulin exocytosis requires Kv2.1 clustering and a direct interaction with syntaxin 1A but is not dependent on its electrical function (Dai et al., 2012; Fu et al., 2017). Consistent with the findings of the previous study (Jensen et al., 2013), we observed a significant reduction in GSIS in INS-1(832/13) cells upon knockdown of Kv2.2. Moreover, knockout of Kv2.2 also reduced GSIS in mouse islets. Kv2.2 channels play a crucial role in maintaining repetitive AP firing by promoting the recovery of voltage-gated sodium channels from inactivation (Johnston et al., 2008). Inhibition of Kv2.2 channels significantly reduces the repetitive firing in medial nucleus of the trapezoid body neurons and cortical pyramidal neurons (Johnston et al., 2008; Wang et al., 2024). In the present study, we found that the major effect of PGE2-induced inhibition of Kv2.2 is to reduce the firing rate in β-cells, suggesting that Kv2.2 plays a key role in the β-cell repetitive firing upon stimulation. The PGE2-induced reduction in β-cell repetitive firing would decrease calcium channel opening, and thus, insulin secretion.

In summary, this study uncovers a previously unknown role of the EP2/4-PKA-Kv2.2 signaling pathway in the inhibitory effect of PGE2 on GSIS in normal β-cells. This provides valuable insights into the complex interplay between prostaglandins, potassium channels, and insulin secretion, contributing to our understanding of pancreatic islet function and potential implications for diabetes mellitus.

Materials and Methods

Ethics statement

All studies were carried out in strict accordance with the recommendations in the Guide for

the Care and Use of Laboratory Animals of the National Institutes of Health. Animal experimental protocols were all approved by the Committee on the Ethics of Animal Experiments of Fudan University. The human pancreatic samples utilized in this study were sourced from the Biobank of Endocrine and Metabolic Diseases. All research procedures were approved by the Ethics Committee of Huashan Hospital, Fudan University, in accordance with the principles of the Helsinki Declaration.

Cell culture

Human embryonic kidney (HEK293T) cells were purchased from the cell bank of the Chinese Academy of Science. HEK293T cells were cultured in DMEM supplemented with 10% fetal bovine serum and 1% penicillin-streptomycin solution. INS-1(832/13) β-cells (Soltani et al., 2011) were cultured in RPMI 1640 with 10% fetal bovine serum, 1% penicillin-streptomycin solution and 0.1% β-mercaptoethanol. All the reagents were purchased from Thermo Fisher Scientific (MA, USA).

Molecular biology

Plasmids for rat Kv2.2 (NM_054000.2) channels in pEGFPN1 vectors were as previously reported (Li et al., 2022). T13D, S14D, T17D, S367D, S448D, S710D, S799D, T801D, S840D, and S448A mutations of the Kv2.2 channel were achieved by PCR-based site-directed mutagenesis using ClonExpress Multis One Step Cloning Kit (Vazyme, Jiangshu, China). All mutations were confirmed by sequencing. HEK293T Cells were transiently transfected with wild-type or mutant Kv2.2 channels for 24 hours using Lipofectamine™ 2000 (Thermo Fisher Scientific, Waltham, MA, USA) before patch clamp recordings. For knockdown plasmids targeting Kv2.2, the shRNA hairpin sequences were inserted into BamHI-HindIII sites of the PAAV-shRNA targeting vector. Oligonucleotides specifying the shRNA are 5′-GGAGCAGATGAACGAAGAACT-3′(KD1-Kv2.2), 5′-GCTGGAGATGCTATACAATGA-3′ (KD2-Kv2.2) and 5′-GCACCCAGTCCGCCCTGAGCAAA-3′ (Scramble). Total RNA extraction and quantitative real-time polymerase chain reaction (qRT-PCR) were performed as previously described (T. Yang et al., 2016). Briefly, qRT-PCR was performed in 20 μL reactions

containing: 2 μL of template, 0.4 μmol/L of each paired primer, and SYBR Green PCR master mix. The thermo-cycling conditions were 94°C, 10 min; 40 cycles of 95°C, 30 s; 55°C, 30 s; 72°C, 60 s; and 72°C, 8 min. Results were normalized by β-actin mRNA. Primers were as previously reported (Hoshino et al., 2007): EP1(forward, reverse): 5′-ACCTTCTTTGGCGGCTCT and 5′- GCACGACACCACCATGATAC; EP2: 5′-CCACCTCATTCTCCTGGCTA and 5′- CGACAACAGAGGACTGAACG; EP3: 5′-AGCTTATGGGGATCATGTGC and 5′- TCTGCTTCTCCGTGTGTGTC; EP4: 5′-TGCGAGTATTCGTCAACCAG and 5′-GGTCTAGGATGGGGTTCACA; β-actin: 5′ -GGACTTCGAGCAAGAGATGG and 5′ -AGCACTGTGTTGGCGTACAG.

Western blot

HEK293T cells were treated with PGE2 for 2, 5 and 10 minutes respectively. HEK293T cell homogenates were prepared using a lysis buffer (20 mM HEPES, 0.5% NP-40, 150 mM NaCl, 10% glycerol, 2 mM EDTA, 50 mM NaF, 0.1 mM Na_3VO_4) with protease inhibitor (P8340, Sigma, USA) and phosphatase inhibitor (P5726, Sigma, USA) cocktail. The protein samples were separated by 10% SDS-PAGE and then transferred to polyvinylidene fluoride membranes (Millipore, USA). The membranes were blocked with 10% non-fat dry milk in Tris-buffered saline with Tween-20 for 1 h at room temperature and then incubated with primary antibodies overnight at 4℃ (anti-phospho-PKA, 1:1000, #5661, Cell Signaling Technology, USA; anti-GAPDH, 1:1000; #AG019, Beyotime, China). The blots were developed using enhanced chemiluminescence reagents and imaged using the ChemiDoc XRS + imaging system from Bio-Rad (Hercules, CA, USA) and manufacturer’s software.

Immunofluorescence

HEK293T and INS-1(832/13) cells were fixed in 4% paraformaldehyde (PFA) for 15 minutes, washed, and blocked (10% donkey serum, 1% BSA) for 2 h at room temperature. Cells were then incubated in primary antibody solution (primary antibody (anti-EP1: 1:200, Ab217925, Abcam, UK; anti-EP2: 1:200, Ab167171, Abcam; anti-EP3: 1:200, Sc-57105, Santa Cruz Biotechnology, TX; anti-EP4: 1:200, Ab217966, Abcam; anti-Kv2.2: 1:200, APC-120, Alomone Labs, IL), 1% horse serum, and 0.3% PBST) for 1 day at 4°C. Cells were washed three times with PBS and incubated overnight at 4°C in a secondary antibody solution

containing Cy3-labeled goat anti-rat IgG or Cy3/FITC-labeled goat anti-mouse/rabbit IgG (1:500, Beyotime), 1% horse serum, and 0.3% PBST. Following another wash with PBS, the cells were treated with DAPI, and imaged using the Nikon A1+ Confocal Microscope System. For mouse and human pancreatic tissue, after overnight treatment in 4% PFA, the tissues were washed three times with PBS and then dehydrated in a fresh 30% sucrose solution. Subsequently, the pancreatic tissue was embedded in OTC compound and sliced into 25 μm sections using a cryostat. Slices were blocked with 10% horse serum and 0.3% PBST for 2 h at room temperature. Following this, the slices underwent the same treatment and imaging procedure as INS-1(832/13) cells described above. The insulin antibody was purchased from Proteintech (1:1000, 66198-1-Ig).

Electrophysiology

Whole-cell potassium currents in HEK293T cells and β-cells were recorded using a Multiclamp 700B amplifier (Molecular Devices, USA). The extracellular solution contained (in mM): 140 NaCl, 2.5 KCl, 10 glucose, 2.5 $CaCl_2$, 10 HEPES, and 1 $MgCl_2$, pH 7.4 adjusted with NaOH. The pipette (2-3 MΩ) solution contained (in mM): 135 K-gluconate, 10 KCl, 1 $CaCl_2$, 1 $MgCl_2$, 10 HEPES, 2 Mg-ATP, and 10 EGTA, pH 7.3 adjusted with KOH. Whole-cell potassium currents were sampled at 10 kHz and filtered at 2 kHz. For β-cell action potential recordings, the extracellular solution contained (in mM): 119 NaCl, 4.7 KCl, 2 $CaCl_2$, 1.2 $MgSO_4$, 1.2 KH_2SO_4, 10 HEPES, pH 7.4 adjusted with NaOH. The pipette solution contained (in mM): 90 KCl, 50 NaCl, 1 $MgCl_2$, 10 EGTA, 10 HEPES, pH 7.3 adjusted with KOH. All of the electrophysiological recordings mentioned above were performed at room temperature.

Isolation of Primary Mouse Pancreatic Islets

Pancreatic islets were isolated from 7-week-old wild-type and KCNB2-KO male mice as previously described (Lernmark, 1974). Briefly, mice were euthanized, and a collagenase XI solution (0.5 mg/ml) was injected into the pancreas via the common bile duct with approximately 3 ml per mouse. The intact pancreas was carefully dissected, and digested for 16 min at 37°C. Afterward, 20 mL of HBSS solution was added, and the mixture was filtered

through a 60-micron sieve. After brief centrifugation, a density gradient centrifugation system was established using Histopaque-1077 (Sigma), Histopaque-1119 (Sigma), and HBSS solution for pancreatic islet separation and purification. The islets were manually picked under a stereo microscope and cultured in RPMI 1640 with 10% fetal bovine serum, 1% penicillin-streptomycin solution. The time between islet isolation and the experiment typically ranged from 24-48 h.

Intraperitoneal glucose tolerance test

Male mice were fasted overnight (16 h) and then injected with D-glucose at a dose of 2.5 g/kg of body weight (intraperitoneal). Blood samples were collected from the tail vein before glucose injection (t = 0) and 15, 30, 60, 90, and 120 minutes after the glucose administration. A 20% glucose solution tailored to each mouse's actual body weight (following the standard of 10 μl/g) was intraperitoneally injected. Glucose levels were measured using a glucometer (Elite, Bayer), following the manufacturer's recommendations. PGE2 (500 μg/kg of body weight) or saline was intraperitoneally injected 1 hour before the glucose administration. The sampling of blood glucose level detection process was carried out in a double-blind fashion.

Insulin secretion assays

For GSIS in INS-1(832/13) cells: INS-1(832/13) cells were cultured in 24-well plates, grown to approximately 90% confluency, washed with PBS, and preincubated for 1 hour in KRB solution (in mM: 120 NaCl, 4.7 KCl, 2.5 $CaCl_2$, 1.2 KH_2PO_4, 1.2 $MgSO_4$, 25 $NaHCO_3$, 10 HEPES) without glucose. The cells were incubated in the KRB solution for an additional 1 hour in the presence of either 2.8 mM or 16.7 mM glucose with or without PGE2, as indicated. Insulin levels in KRB solution were quantified by the Insulin ELISA Kit (Crystal Chem, 90080, USA). For GSIS in islets: islets from 5 WT or KO male mice aged 7 weeks were used. Ten islets per mouse were preincubated in KRB buffer (supplemented with 0.025% BSA, pH 7.4) for 1 hour. Subsequently, the medium was removed, followed by sequential treatment with KRB solution (containing 16.7 mM glucose with or without PGE2) for 1 hour. Insulin in the supernatant was quantified using the same ELISA kit as above.

Generation of Kv2.2 knockout mice

The Kv2.2 channel coding gene, KCNB2 (Accession: NM_001098528.3), underwent conventional knockout using CRISPR-Cas9 gene editing. Two guide RNAs (gRNAs) were designed to target the KCNB2 gene. The sequences for the gRNAs are as follows: gRNA1: GAGAGTTAAGATCAACGTAG; gRNA2: AACTCGTCCGTGGCTGCAAA. The Cas9 protein was prepared and complexed with the two synthesized gRNAs to form ribonucleoprotein complexes. Ribonucleoprotein complexes were microinjected to fertilized C57BL/6 mouse oocytes to induce double-strand breaks at the KCNB2 gene target sites. The microinjected embryos were cultured in vitro to the appropriate developmental stage and then transferred into the oviducts or uteruses of pseudo pregnant recipient female mice. The recipient females gave birth to F_0 offspring. Genotyping of F_0 Mice: DNA was extracted from the tail tips of the F_0 mice. PCR was performed using two pairs of primers to amplify the regions flanking the target sites of the KCNB2 gene. The primer sequences are as follows: F1: TGATGTGGCGATGCCTATTCC; R1: TTCCCACAGACTAACACTTACGG; R2: TCTTCTGATGGTATCTGGCTTGG. The PCR products were purified and sequenced to confirm the knockout of the KCNB2 gene. Mice confirmed to have the desired KCNB2 gene knockout were bred to produce a stable line of KCNB2 conventional knockout mice for further studies. The KCNB2 knockout mouse was created by Cyagen Biosciences (Suzhou) Inc, China. All animals were accommodated in specific pathogen-free Fudan University facilities following a 12-hour light-dark cycle.

Data analysis

The electrophysiological data were analyzed using Clampfit 10.7 (Molecular Devices, USA). Quantitative analysis of the western blot experiments was performed with ImageJ (v1.53, NIH, USA). Data are given as the mean ± SEM. Two-tailed paired or unpaired *t*-test was used to compare two samples, and one-way ANOVA with Bonferroni *post hoc* test was employed for the comparison of multiple samples. A p-value < 0.05 was considered significant. All statistical analyses were performed using GraphPad Prism (v9.4, GraphPad Software Inc, USA).

Conflict of Interest Statement

The authors declare no competing financial interests.

Author contributions

Chengfang Pan, Ying Liu: Investigation, Formal analysis, Writing – review & editing. Liangya Wang, Yunzhi Ni, Wengyong Fan, Xuefeng Zhang, Chenyang Li, Di Wu: Investigation. Jin Li: Writing – review & editing. Zhaoyang Li: Conceptualization, Investigation. Rui Liu: Supervision, Writing –review & editing. Changlong Hu: Conceptualization, Supervision, Writing – original draft, Writing –review & editing.

Acknowledgement

This work was supported d by the National Key Research & Development Program of China (2022YFC3602700&2022YFC3602702), the Science and Technology Innovation 2030 - Brain Science and Brain- Inspired Intelligence Project (2021ZD0201301), the Natural Science Foundation of Shanghai (23ZR1425900), the National Natural Science Foundation of China (31771282; 32200797).

Data Availability Statement

All data supporting the findings of this study are available within the paper and its Supplementary Information.

References

Blodgett, D. M., Nowosielska, A., Afik, S., Pechhold, S., Cura, A. J., Kennedy, N. J., . . . diIorio, P. (2015). Novel Observations From Next-Generation RNA Sequencing of Highly Purified Human Adult and Fetal Islet Cell Subsets. *Diabetes, 64*(9), 3172-3181. doi:10.2337/db15-0039

Bramswig, N. C., Everett, L. J., Schug, J., Dorrell, C., Liu, C., Luo, Y., . . . Kaestner, K. H. (2013). Epigenomic plasticity enables human pancreatic alpha to beta cell reprogramming. *J Clin Invest, 123*(3), 1275-1284. doi:10.1172/JCI66514

Braun, M., Ramracheya, R., Bengtsson, M., Zhang, Q., Karanauskaite, J., Partridge, C., . . . Rorsman, P. (2008). Voltage-gated ion channels in human pancreatic beta-cells: electrophysiological characterization and role in insulin secretion. *Diabetes, 57*(6), 1618-1628. doi:10.2337/db07-0991

Carboneau, B. A., Breyer, R. M., & Gannon, M. (2017). Regulation of pancreatic β-cell function and mass dynamics by prostaglandin signaling. *J Cell Commun Signal, 11*(2), 105-116. doi:10.1007/s12079-017-0377-7

Ceddia, R. P., Lee, D., Maulis, M. F., Carboneau, B. A., Threadgill, D. W., Poffenberger, G., . . . Breyer, R. M. (2016). The PGE2 EP3 Receptor Regulates Diet-Induced Adiposity in Male Mice. *Endocrinology, 157*(1), 220-232. doi:10.1210/en.2015-1693

Corboz, M. R., Salvail, W., Gagnon, S., LaSala, D., Laurent, C. E., Salvail, D., . . . Chapman, R. W. (2021). Prostanoid receptor subtypes involved in treprostinil-mediated vasodilation of rat pulmonary arteries and in treprostinil-mediated inhibition of collagen gene expression of human lung fibroblasts. *Prostaglandins Other Lipid Mediat, 152*, 106486. doi:10.1016/j.prostaglandins.2020.106486

Dai, X. Q., Manning Fox, J. E., Chikvashvili, D., Casimir, M., Plummer, G., Hajmrle, C., . . . Macdonald, P. E. (2012). The voltage-dependent potassium channel subunit Kv2.1 regulates insulin secretion from rodent and human islets independently of its electrical function. *Diabetologia, 55*(6), 1709-1720. doi:10.1007/s00125-012-2512-6

Dickerson, M. T., Dadi, P. K., Zaborska, K. E., Nakhe, A. Y., Schaub, C. M., Dobson, J. R., . . . Jacobson, D. A. (2022). G(i/o) protein-coupled receptor inhibition of beta-cell electrical excitability and insulin secretion depends on Na(+)/K(+) ATPase activation. *Nat Commun, 13*(1), 6461. doi:10.1038/s41467-022-34166-z

Drews, G., Krippeit-Drews, P., & Dufer, M. (2010). Electrophysiology of islet cells. *Adv Exp Med Biol, 654*, 115-163. doi:10.1007/978-90-481-3271-3_7

Fenske, R. J., Weeks, A. M., Daniels, M., Nall, R., Pabich, S., Brill, A. L., . . . Kimple, M. E. (2022). Plasma Prostaglandin E(2) Metabolite Levels Predict Type 2 Diabetes Status and One-Year Therapeutic Response Independent of Clinical Markers of Inflammation. *Metabolites, 12*(12). doi:10.3390/metabo12121234

Fox, P. D., Loftus, R. J., & Tamkun, M. M. (2013). Regulation of Kv2.1 K Conductance by Cell Surface Channel Density. *Journal of Neuroscience, 33*(3), 1259-1270. doi:10.1523/Jneurosci.3008-12.2013

Fu, J., Dai, X., Plummer, G., Suzuki, K., Bautista, A., Githaka, J. M., . . . MacDonald, P. E. (2017). Kv2.1 Clustering Contributes to Insulin Exocytosis and Rescues Human β-Cell Dysfunction. *Diabetes, 66*(7), 1890-1900. doi:10.2337/db16-1170

Greitzer-Antes, D., Xie, L., Qin, T., Xie, H., Zhu, D., Dolai, S., . . . Gaisano, H. Y. (2018). K(v)2.1 clusters on β-cell plasma membrane act as reservoirs that replenish pools of newcomer insulin granule through their interaction with syntaxin-3. *J Biol Chem, 293*(18), 6893-6904. doi:10.1074/jbc.RA118.002703

He, X., Smith, S. E., Chen, S., Li, H., Wu, D., Meneses-Giles, P. I., . . . Li, L. (2021). Tumor-initiating stem cell shapes its microenvironment into an immunosuppressive barrier

and pro-tumorigenic niche. *Cell Rep, 36*(10), 109674. doi:10.1016/j.celrep.2021.109674

Hoshino, T., Nakaya, T., Homan, T., Tanaka, K., Sugimoto, Y., Araki, W., . . . Mizushima, T. (2007). Involvement of prostaglandin E2 in production of amyloid-beta peptides both in vitro and in vivo. *J Biol Chem, 282*(45), 32676-32688. doi:10.1074/jbc.M703087200

Jacobson, D. A., Kuznetsov, A., Lopez, J. P., Kash, S., Ammälä, C. E., & Philipson, L. H. (2007). Kv2.1 ablation alters glucose-induced islet electrical activity, enhancing insulin secretion. *Cell Metab, 6*(3), 229-235. doi:10.1016/j.cmet.2007.07.010

Jensen, M. V., Haldeman, J. M., Zhang, H., Lu, D., Huising, M. O., Vale, W. W., . . . Newgard, C. B. (2013). Control of voltage-gated potassium channel Kv2.2 expression by pyruvate-isocitrate cycling regulates glucose-stimulated insulin secretion. *J Biol Chem, 288*(32), 23128-23140. doi:10.1074/jbc.M113.491654

Johnston, J., Griffin, S. J., Baker, C., Skrzypiec, A., Chernova, T., & Forsythe, I. D. (2008). Initial segment Kv2.2 channels mediate a slow delayed rectifier and maintain high frequency action potential firing in medial nucleus of the trapezoid body neurons. *J Physiol, 586*(14), 3493-3509. doi:10.1113/jphysiol.2008.153734

Kimple, M. E., Keller, M. P., Rabaglia, M. R., Pasker, R. L., Neuman, J. C., Truchan, N. A., . . . Attie, A. D. (2013). Prostaglandin E2 receptor, EP3, is induced in diabetic islets and negatively regulates glucose- and hormone-stimulated insulin secretion. *Diabetes, 62*(6), 1904-1912. doi:10.2337/db12-0769

Ku, G. M., Kim, H., Vaughn, I. W., Hangauer, M. J., Myung Oh, C., German, M. S., & McManus, M. T. (2012). Research resource: RNA-Seq reveals unique features of the pancreatic beta-cell transcriptome. *Mol Endocrinol, 26*(10), 1783-1792. doi:10.1210/me.2012-1176

Lernmark, A. (1974). The preparation of, and studies on, free cell suspensions from mouse pancreatic islets. *Diabetologia, 10*(5), 431-438. doi:10.1007/BF01221634

Li, Z., Dong, W., Zhang, X., Lu, J. M., Mei, Y. A., & Hu, C. (2022). Protein Kinase C Controls the Excitability of Cortical Pyramidal Neurons by Regulating Kv2.2 Channel Activity. *Neurosci Bull, 38*(2), 135-148. doi:10.1007/s12264-021-00773-x

Liu, P. W., & Bean, B. P. (2014). Kv2 channel regulation of action potential repolarization and firing patterns in superior cervical ganglion neurons and hippocampal CA1 pyramidal neurons. *J Neurosci, 34*(14), 4991-5002. doi:10.1523/JNEUROSCI.1925-13.2014

MacDonald, P. E., Sewing, S., Wang, J., Joseph, J. W., Smukler, S. R., Sakellaropoulos, G., . . . Wheeler, M. B. (2002). Inhibition of Kv2.1 voltage-dependent K+ channels in pancreatic beta-cells enhances glucose-dependent insulin secretion. *J Biol Chem, 277*(47), 44938-44945. doi:10.1074/jbc.M205532200

Meng, Z. X., Sun, J. X., Ling, J. J., Lv, J. H., Zhu, D. Y., Chen, Q., . . . Han, X. (2006).

Prostaglandin E2 regulates Foxo activity via the Akt pathway: implications for pancreatic islet beta cell dysfunction. *Diabetologia, 49*(12), 2959-2968. doi:10.1007/s00125-006-0447-5

Neuman, J. C., Schaid, M. D., Brill, A. L., Fenske, R. J., Kibbe, C. R., Fontaine, D. A., . . . Kimple, M. E. (2017). Enriching Islet Phospholipids With Eicosapentaenoic Acid Reduces Prostaglandin E(2) Signaling and Enhances Diabetic β-Cell Function. *Diabetes, 66*(6), 1572-1585. doi:10.2337/db16-1362

Oshima, H., Taketo, M. M., & Oshima, M. (2006). Destruction of pancreatic beta-cells by transgenic induction of prostaglandin E2 in the islets. *J Biol Chem, 281*(39), 29330-29336. doi:10.1074/jbc.M602424200

Parazzoli, S., Harmon, J. S., Vallerie, S. N., Zhang, T., Zhou, H., & Robertson, R. P. (2012). Cyclooxygenase-2, not microsomal prostaglandin E synthase-1, is the mechanism for interleukin-1β-induced prostaglandin E2 production and inhibition of insulin secretion in pancreatic islets. *J Biol Chem, 287*(38), 32246-32253. doi:10.1074/jbc.M112.364612

Shridas, P., Zahoor, L., Forrest, K. J., Layne, J. D., & Webb, N. R. (2014). Group X secretory phospholipase A2 regulates insulin secretion through a cyclooxygenase-2-dependent mechanism. *J Biol Chem, 289*(40), 27410-27417. doi:10.1074/jbc.M114.591735

Soltani, N., Qiu, H., Aleksic, M., Glinka, Y., Zhao, F., Liu, R., . . . Wang, Q. (2011). GABA exerts protective and regenerative effects on islet beta cells and reverses diabetes. *Proc Natl Acad Sci U S A, 108*(28), 11692-11697. doi:10.1073/pnas.1102715108

Srinivasalu, N., Zhang, S., Xu, R., Reinach, P. S., Su, Y., Zhu, Y., . . . Zhou, X. (2020). Crosstalk between EP2 and PPARalpha Modulates Hypoxic Signaling and Myopia Development in Guinea Pigs. *Invest Ophthalmol Vis Sci, 61*(8), 44. doi:10.1167/iovs.61.8.44

Sugimoto, Y., & Narumiya, S. (2007). Prostaglandin E receptors. *J Biol Chem, 282*(16), 11613-11617. doi:10.1074/jbc.R600038200

Tamarina, N. A., Kuznetsov, A., Fridlyand, L. E., & Philipson, L. H. (2005). Delayed-rectifier (KV2.1) regulation of pancreatic beta-cell calcium responses to glucose: inhibitor specificity and modeling. *Am J Physiol Endocrinol Metab, 289*(4), E578-585. doi:10.1152/ajpendo.00054.2005

Tran, P. O., Gleason, C. E., & Robertson, R. P. (2002). Inhibition of interleukin-1beta-induced COX-2 and EP3 gene expression by sodium salicylate enhances pancreatic islet beta-cell function. *Diabetes, 51*(6), 1772-1778. doi:10.2337/diabetes.51.6.1772

Truchan, N. A., Fenske, R. J., Sandhu, H. K., Weeks, A. M., Patibandla, C., Wancewicz, B., . . . Kimple, M. E. (2021). Human Islet Expression Levels of Prostaglandin E(2) Synthetic Enzymes, But Not Prostaglandin EP3 Receptor, Are Positively Correlated with Markers of β-Cell Function and Mass in Nondiabetic Obesity. *ACS Pharmacol Transl Sci, 4*(4), 1338-1348. doi:10.1021/acsptsci.1c00045

Vennemann, A., Gerstner, A., Kern, N., Ferreiros Bouzas, N., Narumiya, S., Maruyama, T., & Nüsing, R. M. (2012). PTGS-2-PTGER2/4 signaling pathway partially protects from diabetogenic toxicity of streptozotocin in mice. *Diabetes, 61*(7), 1879-1887. doi:10.2337/db11-1396

Wang, Y., Zhang, Y., Hu, J., Pan, C., Gao, Y., Liu, Q., . . . Hu, C. (2024). Glucocorticoids modulate neural activity via a rapid non-genomic effect on Kv2.2 channels in the central nervous system. *Neurobiol Stress, 28,* 100593. doi:10.1016/j.ynstr.2023.100593

Yang, S. N., Shi, Y., Yang, G., Li, Y., Yu, J., & Berggren, P. O. (2014). Ionic mechanisms in pancreatic β cell signaling. *Cell Mol Life Sci, 71*(21), 4149-4177. doi:10.1007/s00018-014-1680-6

Yang, T., Zhang, H. L., Liang, Q., Shi, Y., Mei, Y. A., Barrett, P. Q., & Hu, C. (2016). Small-Conductance Ca2+-Activated Potassium Channels Negatively Regulate Aldosterone Secretion in Human Adrenocortical Cells. *Hypertension, 68*(3), 785-795. doi:10.1161/HYPERTENSIONAHA.116.07094

Zhou, P., Qian, L., Chou, T., & Iadecola, C. (2008). Neuroprotection by PGE2 receptor EP1 inhibition involves the PTEN/AKT pathway. *Neurobiol Dis, 29*(3), 543-551. doi:10.1016/j.nbd.2007.11.010

Figure legends

Figure 1. PGE2 inhibits Kv2.2 channels in HEK293T cells.

(A) Representative Kv2.2 current traces induced by a depolarization pulse from -80 to +40 mV under the control condition (black) and subsequently in the presence of 10 μM PGE2 (red) in the same HEK293T cell. PGE2 was applied to the extracellular solution and recordings taken at an interval of 10 s. **(B)** The time course of the Kv2.2 current inhibition by 10 μM PGE2. **(C)** PGE2 inhibited Kv2.2 currents in a concentration-dependent manner. n.s., not significant. ***$p < 0.001$. One-way ANOVA with Bonferroni *post hoc* test (0.01 μM: $n = 7$, $p = 0.4002$; 0.1 μM: $n = 8$, $p = 0.0672$; 1 μM: $n = 9$, $p = 0.0002$; 10 μM: $n = 24$, $p < 0.0001$; 100 μM: $n = 17$, $p < 0.0001$). **(D)** Left, representative Kv2.2 current recordings in response to 200-ms 10-mV depolarizing steps from -80 to +50 mV in the control (top, black) and PGE2-treated (bottom, red) groups. Right, plot of the current-voltage relationship from Left ($n = 7$ for each data point). *$p < 0.05$. Two-tailed paired *t*-test. **(E)** Plot of Kv2.2 current activation curves in the control

(black) and PGE2-treated (red, n = 7 for each data point) groups. **(F)** Plot of Kv2.2 current inactivation curves in the control (black) and PGE2-treated (red, n = 7 for each data point) groups.

Figure 2. PGE2 inhibits Kv2.2 currents via the EP2/EP4 signaling pathway in HEK293T cells.

(A) Top**,** RT-PCR showing the mRNA expression of EP1-4 receptors in HEK293T cells. Bottom, statistics of the mRNA expression of EP1-4 receptors in HEK293T cells (n = 4). **(B)** Representative examples of immunofluorescence images showing expression of EP1-4 receptors in HEK293T cells. Scale bar, 20 μm. **(C)** SC51089 (the EP1 receptor antagonist), AH6809 (the EP2 receptor antagonist), L798106 (the EP3 receptor antagonist), and AH23848 (the EP4 receptor antagonist) per se did not alter Kv2.2 currents. n.s., not significant (SC51089: n = 8, p = 0.9154; AH6809: n = 10, p = 0.0661; L798106: n = 9, p = 0.5581; AH23848: n = 6, p = 0.8827). **(D)** Representative Kv2.2 current traces induced by a depolarization pulse from -80 to +40 mV in the presence of SC51089, AH6809, L798106 and AH23848 respectively, and subsequently in the presence of an additional 10 μM PGE2 in the same HEK293T cell. **(E)** Statistical analysis showing the effect of EP1-4 antagonists on PGE2-induced inhibition of Kv2.2 channels. ****P < 0.001 versus PGE2 alone by a two-tailed unpaired *t*-test. n.s., not significant. (+SC51089: n = 5, p = 0.3997; +AH6809: n = 10, p < 0.0001; +L798106: n = 6, p = 0.1785; +AH23848: n = 8, p < 0.0001). **(F)** Left, representative Kv2.2 current traces induced by a depolarization pulse from -80 to +40 mV under the control condition and subsequently in the presence of the EP2 receptor agonist Butaprost in the same HEK293T cell. Right, statistics for the amplitude of Kv2.2 currents from Left using a two-tailed paired *t*-test (n = 5). *p = 0.0306. **(G)** Similar to F, but with the EP4 receptor agonist CAY10598 in the extracellular solution (n = 8). ***p = 0.0003.

Figure 3. PGE2 inhibits Kv2.2 currents via the PKA signaling pathway.

(A) Top, representative western blot showing the PKA phosphorylation level in HEK293T cells following treatment with 10 μM PGE2 for time intervals of 2, 5, and 10 minutes. Bottom, statistics from three independent experiments using a one-way ANOVA with Bonferroni *post hoc* test (2 min: **p = 0.0078; 5 min: **p = 0.002; 10 min: ***p = 0.0002). **(B)** Top,

representative Kv2.2 current traces induced by a depolarization pulse from -80 to +40 mV under the control condition (black) and subsequently in the presence of 10 μM Db-cAMP (red) in the same HEK293T cell. Bottom, statistics for the amplitude of Kv2.2 currents from Top using a two-tailed paired *t*-test (n = 6, **p = 0.0035). **(C)** Similar to B, but with Rp-cAMP in the extracellular solution (n = 8, p = 0.3851). **(D)** Top, representative Kv2.2 current traces induced by a depolarization pulse from -80 to +40 mV in the presence of 10 μM Rp-cAMP (black) and subsequently in the presence of an additional 10 μM PGE2 (red) in the same HEK293T cell. Bottom, statistics for the amplitude of Kv2.2 current from Top using a two-tailed paired *t*-test (n = 5, p = 0.6425). n.s., not significant. **(E)** Schematic structural models of Kv2.2 channels indicate the positions of nine potential PKA phosphorylation sites. **(F)** Statistics for the amplitude of wild-type and various mutant Kv2.2 channel currents, induced by a depolarization pulse from -80 to +40 mV (n = 6-24). ****P < 0.0001 compared to wild-type Kv2.2 by a one-way ANOVA with Bonferroni *post hoc* test. **(G)** Left**,** representative Kv2.2-S448D mutant channel current traces induced by a depolarization pulse from -80 to +40 mV under the control condition (black) and subsequently in the presence of 10 μM PGE2 (red) in the same HEK293T cell. Right, statistics for the amplitude of Kv2.2 current from Left using a two-tailed paired *t*-test (n = 6, p > 0.9999). n.s., not significant. **(H)** Similar to G**,** this section presents data for the Kv2.2S448A mutant channel in HEK293T cells (n = 6, p > 0.9999).

Figure 4. PGE2 inhibits native Kv2.2 channels in INS-1(832/13) cells.

(A) Representative examples of immunofluorescence images showing high expression of Kv2.2 channels in INS-1(832/13) cells. Scale bar, 20 μm. **(B)** Left, representative I_K traces induced by a depolarization pulse from -80 to +40 mV under the control condition (black) and subsequently in the presence of 10 μM PGE2 (red) in the same INS-1(832/13) cell. Right, statistics for the amplitude of I_K from Left using a two-tailed paired *t*-test (n =10, ****P < 0.0001). **(C)** Left, representative examples of western blot images showing the effects of the two shRNA oligos (KD1-Kv2.2 and KD2-Kv2.2) on Kv2.2 channel surface expression in HEK293T cells transfected with Kv2.2. Right, statistics for cell surface expression of Kv2.2 channels from Left using a two-tailed unpaired *t*-test. KD1-Kv2.2: n = 7, **p = 0.0066; KD2-Kv2.2: n = 7, ****p < 0.0001; KD1/KD2-Kv2.2: n=3, ***p = 0.0005, compared with

scramble. **(D)** Knockdown of Kv2.2 channels significantly reduced I_K amplitude in INS-1(832/13) cells (n = 6, *p < 0.05). **(E)** Left, representative I_K traces induced by a depolarization pulse from -80 to +40 mV under the control condition (black) and subsequently in the presence of 10 μM PGE2 (red) in the same INS-1(832/13) cell transfected with scramble control or KD2-Kv2.2. **(F)** Knockdown of Kv2.2 channels abrogated the inhibitory effect of PGE2 on I_K in INS-1(832/13) cells. Scramble-PGE2: n =11, ****p < 0.0001; KD2-PGE2: n = 6, p = 0.1227; two-tailed paired *t*-test. **(G)** Left, representative Kv2.2 current traces induced by a depolarization pulse from -80 to +40 mV under the control condition and subsequently in the presence of the EP2 receptor agonist Butaprost in the same INS-1(832/13) cell. Right, statistics for the amplitude of Kv2.2 currents from Left using a two-tailed paired *t*-test (n = 10, ****P < 0.0001). **(H)** Similar to G, but with the EP4 receptor agonist CAY10598 in the extracellular solution (n = 9, ****P < 0.0001).

Figure 5. PGE2 reduces β-cell electrical excitability through Kv2.2 channels.

(A) Left, representative action potential (AP) firings induced by 20 mM glucose under the control condition and subsequently in the presence of 10 μM PGE2 in the same INS-1(832/13) cell. Right, statistics for the AP firing frequency (*p = 0.0385), amplitude (p = 0.9478), and half-width (* p = 0.0101) from A (n = 9). Two-tailed paired *t*-test. **(B)** Similar to A, but the INS-1(832/13) cells were transfected with scramble-Kv2.2 (n = 8) (frequency: *p = 0.0285; amplitude: p = 0.6603; half-width: *p = 0.0281. **(C)** Similar to B, but the INS-1(832/13) cells were transfected with KD2-Kv2.2 (n = 6). n.s., not significant (frequency: p = 0.4564; amplitude: p = 0.1601; half-width: p = 0.3034). **(D)** Representative immunofluorescence images showing expression of EP1-4 receptors in INS-1(832/13) cells. Scale bar, 20 μm. **(E)** Representative immunofluorescence images showing expression of EP1-4 receptors in mouse and human islets. Scale bar, 20 μm.

Figure 6. PGE2 reduces β-cell electrical excitability through EP2/4.

(A) Top, representative AP firings induced by 20 mM glucose under the control condition and subsequently in the presence of 20 μM Butaprost in the same INS-1(832/13) cell. Bottom, statistics for the AP firing frequency (*p = 0.0312), amplitude (p = 0.7354), and half-width (p

= 0.2067) from Top (n = 6). Two-tailed paired *t*-test. **(B)** Similar to A, but in the presence of 20 μM CAY10598(n = 6), AP firing frequency (*p = 0.0291), amplitude (p= 0.2211), half-width (p = 0.0753).

Figure 7. PGE2 inhibits glucose-stimulated insulin secretion (GSIS) through Kv2.2 channels.

(A) Effects of PGE2 on insulin secretion in INS-1(832/13) cells under basal (2.8 mM, 2.8 G) or stimulatory (16.7 mM, 16.7 G) glucose concentrations (n = 3). 2.8G, PGE2: n.s., not significant (p = 0.9497); 16.7G, PGE2: **p = 0.0082. Two-tailed unpaired *t*-test. **(B)** Knockdown of Kv2.2 channels reduced GIGS and greatly alleviated the PGE2-induced inhibition of GSIS in INS-1(832/13) cells (n = 3). ****P < 0.0001; n.s., not significant. Two-tailed unpaired *t*-tests. **(C)** Top, cartoon of the Kv2.2 targeted gene disruption. Bottom, PCR products generated from wild-type (+/+, 521 bp), heterozygous (+/−, 521 bp and 415 bp), and homozygous knockout (−/−, 415 bp) mice with primers (F1 and R1) specific to the surrounding Kv2.2 gene disruption sequence and one primer (R2) specific to the targeting sequence. NTC, no template control. **(D)** Representative immunofluorescence images showing expression of Kv2.2 channels in wild-type and Kv2.2$^{-/-}$ knockout mouse pancreatic islet β-cells. Scale bar, 20 μm. **(E)** Kv2.2 knockout did not alter the body weight of animals. **(F)** Left, the effect of PGE2 on the glucose tolerance test in Kv2.2$^{-/-}$, and control animals. N = 4 animals per group. Right, statistics for AUC from Left. ** P = 0.0064. n.s., not significant (p = 0.9684). Two-tailed unpaired *t*-tests. **(G)** Statistics for the effect of PGE2 on GSIS (16.7 mM glucose) in isolated islets from Kv2.2$^{-/-}$, and control animals. N = 5 animals per group. * P = 0.0483, ** P = 0.001. n.s., not significant (p = 0.4766). Two-tailed unpaired *t*-tests.

Figure 8. PGE2 inhibits mouse pancreatic β-cell electrical excitability through Kv2.2 channels.

(A) Left, representative I_K recordings in response to 200-ms depolarization pulses from - 80 to +50 mV in wild-type and Kv2.2$^{-/-}$ knockout mouse pancreatic β-cells. Right, plot of the current-voltage relationship from Left (n = 7 for each data point). **(B)** Left, representative I_K traces induced by a depolarization pulse from -80 to +40 mV under the control condition and

subsequently in the presence of 10 μM PGE2 in the same β-cell from wild-type or Kv2.2$^{-/-}$ mice. Right, statistics for the I_K amplitude using a two-tailed paired *t*-test. ****P < 0.0001, n = 17; n.s., not significant (p = 0.6317, n= 12). **(C)** Left, representative AP firings induced by 20 mM glucose under the control condition and subsequently in the presence of 10 μM PGE2 in the same β-cell within wild-type mouse pancreatic islets. Right, statistics for the AP firing frequency (*p = 0.0288), amplitude (p =0.8589), and half-width (p = 0.0563) from Left (n = 4). Two-tailed paired *t*-tests. **(D)** Left, representative AP firings induced by 20 mM glucose under the control condition and subsequently in the presence of 10 μM PGE2 in the same β-cell within Kv2.2$^{-/-}$ mouse pancreatic islets. Right, statistics for the AP firing frequency (p = 0.1536), amplitude (p = 0.1981), and half-width (p = 0.2385) from Left (n =3). Two-tailed paired *t*-tests.

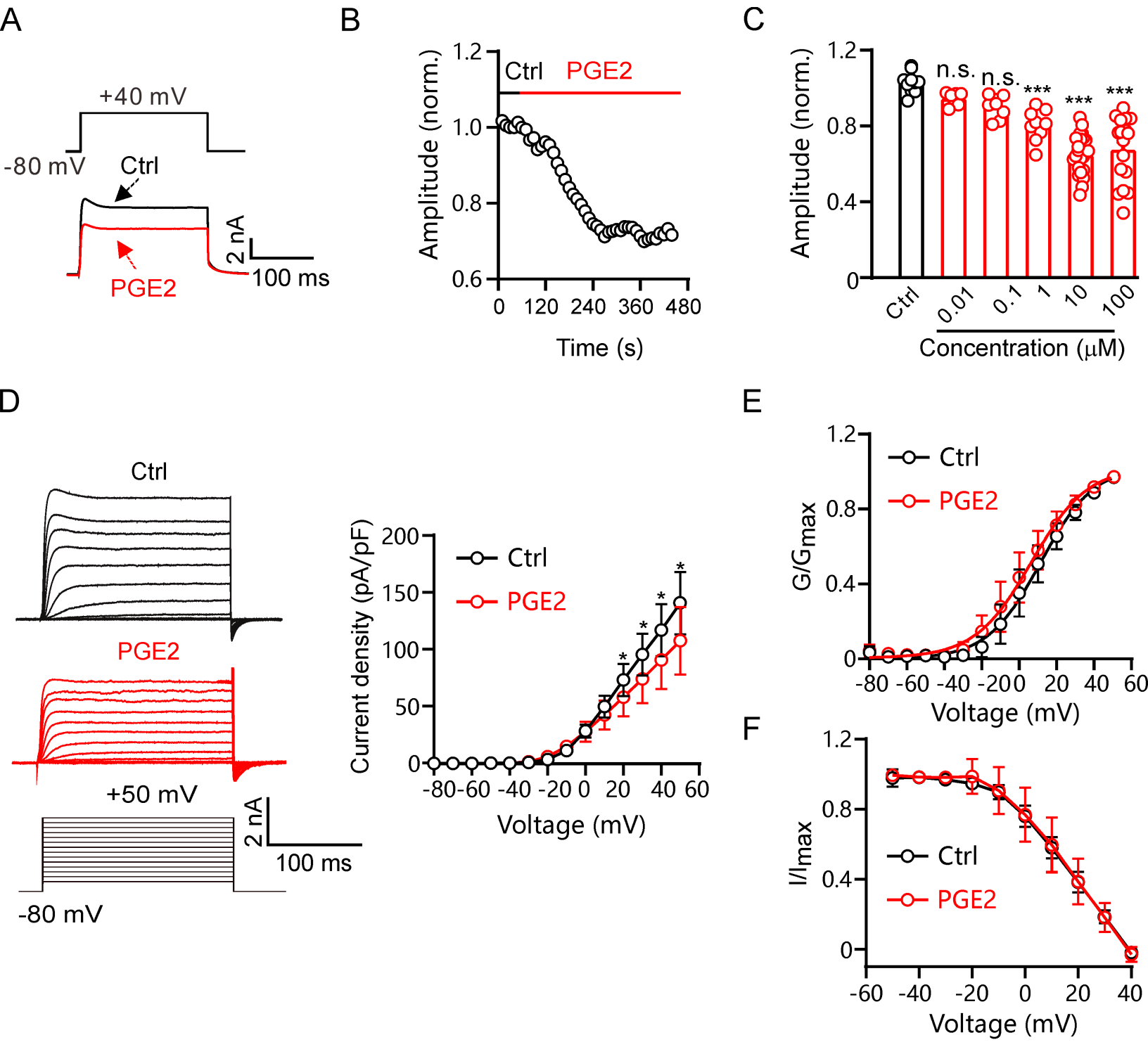
A
+40 mV
-80 mV
Ctrl
PGE2
2 nA
100 ms
B
Ctrl
PGE2
Amplitude (norm.)
1.2
1.0
0.8
0.6
0
120
240
360
480
Time (s)
C
Amplitude (norm.)
1.2
0.8
0.4
0
n.s.
n.s.
***
***
***
Ctrl
0.01
0.1
1
10
100
Concentration (μM)
D
Ctrl
PGE2
+50 mV
-80 mV
2 nA
100 ms
Current density (pA/pF)
200
150
100
50
0
Ctrl
PGE2
-80
-60
-40
-20
0
20
40
60
Voltage (mV)
E
G/Gmax
1.2
0.8
0.4
0
Ctrl
PGE2
-80
-60
-40
-20
0
20
40
60
Voltage (mV)
F
I/Imax
1.2
0.8
0.4
0
Ctrl
PGE2
-60
-40
-20
0
20
40
Voltage (mV)

Fig. 1

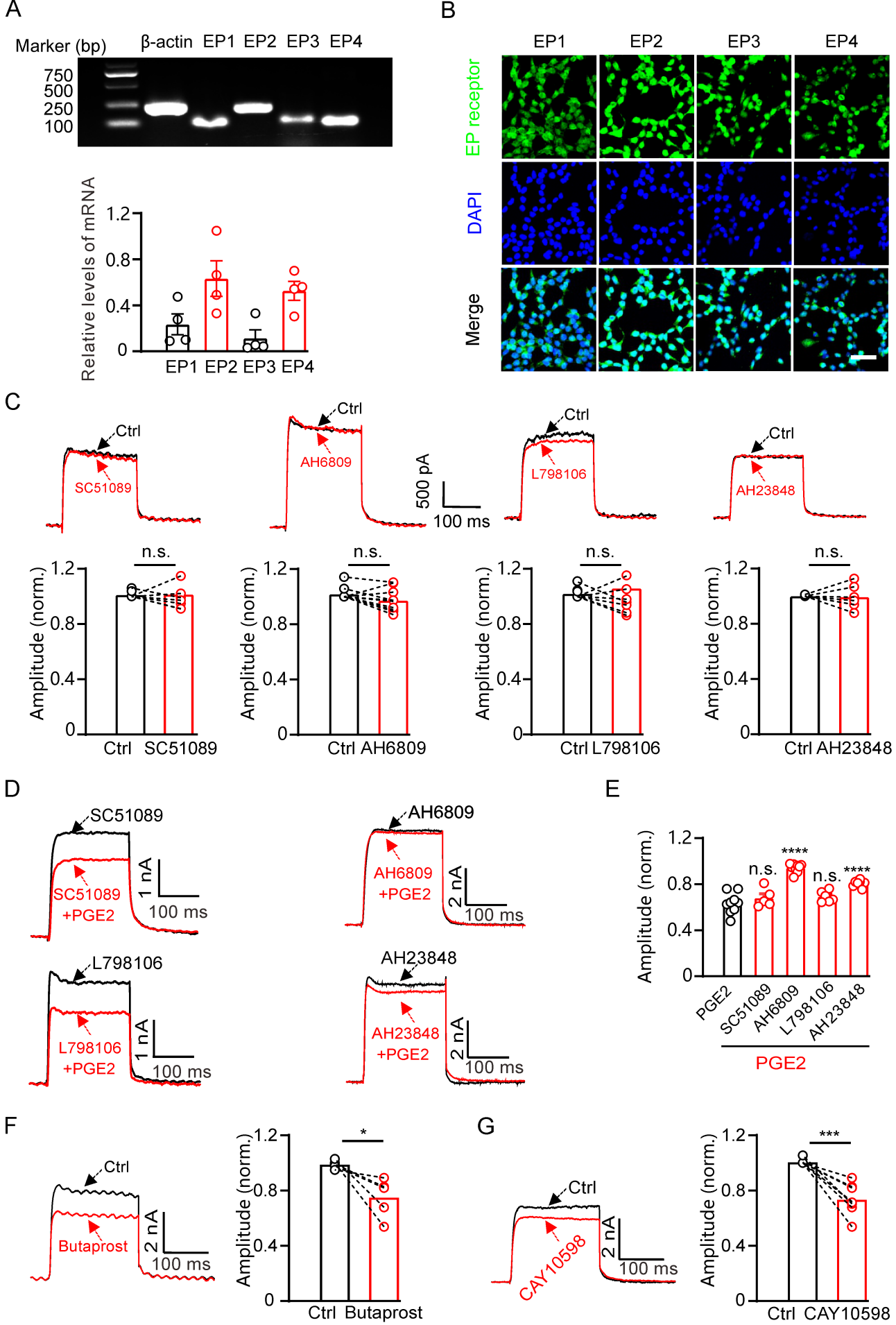
A
Marker (bp)
β-actin EP1 EP2 EP3 EP4
750
500
250
100
Relative levels of mRNA
1.2
0.8
0.4
0
EP1 EP2 EP3 EP4
B
EP1 EP2 EP3 EP4
EP receptor
DAPI
Merge
C
Ctrl
SC51089
AH6809
L798106
AH23848
500 pA
100 ms
n.s.
Amplitude (norm.)
Ctrl SC51089
Ctrl AH6809
Ctrl L798106
Ctrl AH23848
D
SC51089
SC51089 +PGE2
1 nA
100 ms
AH6809
AH6809 +PGE2
2 nA
L798106
L798106 +PGE2
AH23848
AH23848 +PGE2
E
****
PGE2
SC51089
AH6809
L798106
AH23848
F
Butaprost
*
Ctrl Butaprost
G
CAY10598
***
Ctrl CAY10598

Fig. 2

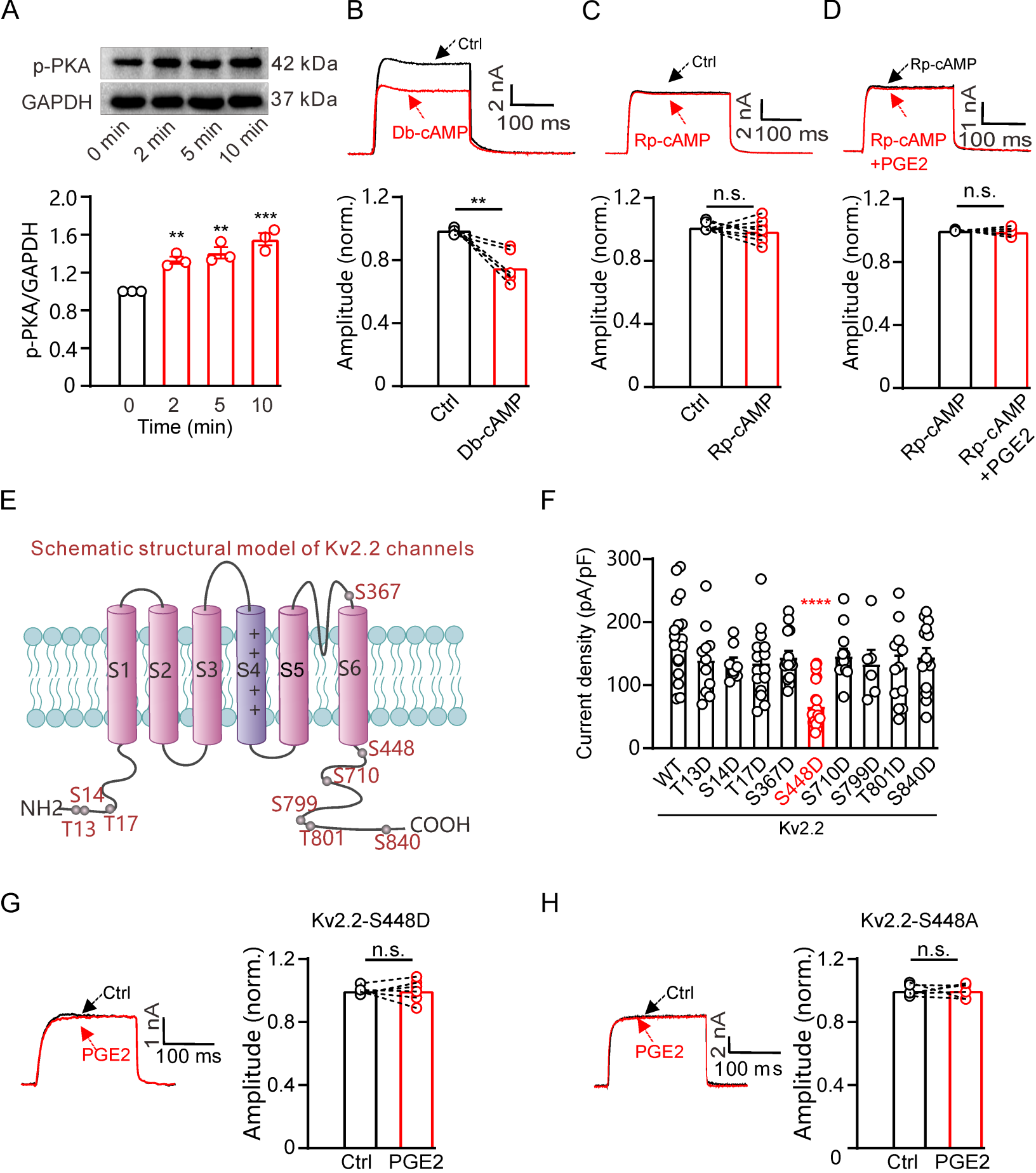
A
p-PKA
GAPDH
42 kDa
37 kDa
0 min
2 min
5 min
10 min
p-PKA/GAPDH
Time (min)
B
Ctrl
Db-cAMP
2 nA
100 ms
Amplitude (norm.)
Ctrl
Db-cAMP
C
Ctrl
Rp-cAMP
2 nA
100 ms
n.s.
D
Rp-cAMP
Rp-cAMP +PGE2
1 nA
100 ms
E
Schematic structural model of Kv2.2 channels
S1
S2
S3
S4
S5
S6
S367
S448
S710
S799
S840
S14
T13
T17
T801
NH2
COOH
F
Current density (pA/pF)
WT
T13D
S14D
T17D
S367D
S448D
S710D
S799D
T801D
S840D
Kv2.2
G
Kv2.2-S448D
PGE2
1 nA
100 ms
Ctrl
PGE2
H
Kv2.2-S448A
PGE2
2 nA
100 ms

Fig. 3

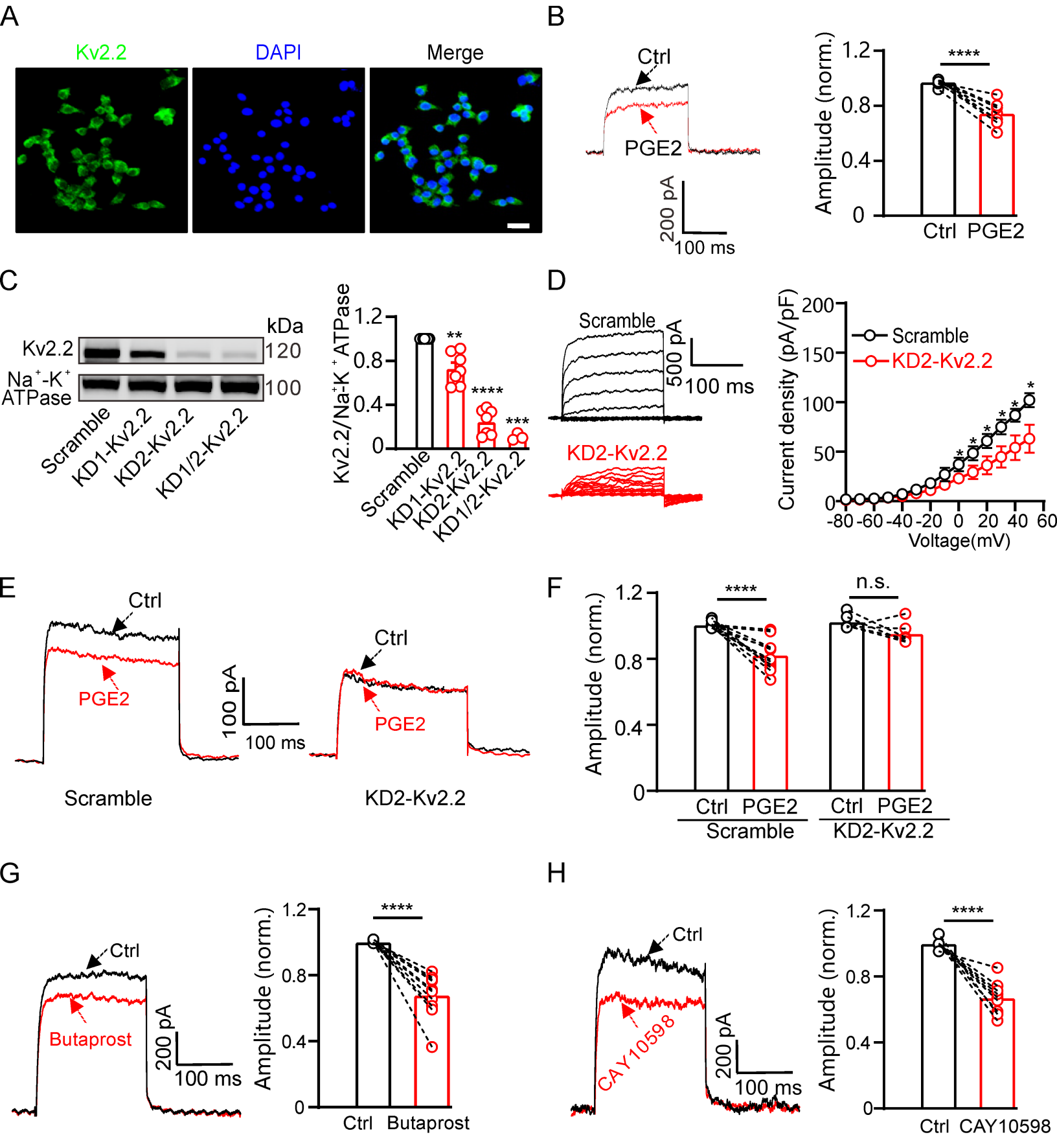
A
Kv2.2
DAPI
Merge
B
Ctrl
PGE2
200 pA
100 ms
Amplitude (norm.)
****
Ctrl
PGE2
C
kDa
Kv2.2
120
Na+-K+ ATPase
100
Scramble
KD1-Kv2.2
KD2-Kv2.2
KD1/2-Kv2.2
Kv2.2/Na+-K+ATPase
**
****
***
D
Scramble
500 pA
100 ms
KD2-Kv2.2
Current density (pA/pF)
Scramble
KD2-Kv2.2
Voltage(mV)
E
Ctrl
PGE2
100 pA
100 ms
Scramble
KD2-Kv2.2
F
Amplitude (norm.)
****
n.s.
Ctrl
PGE2
Scramble
KD2-Kv2.2
G
Ctrl
Butaprost
200 pA
100 ms
Amplitude (norm.)
****
Ctrl
Butaprost
H
Ctrl
CAY10598
200 pA
100 ms
Amplitude (norm.)
****
Ctrl
CAY10598

Fig. 4

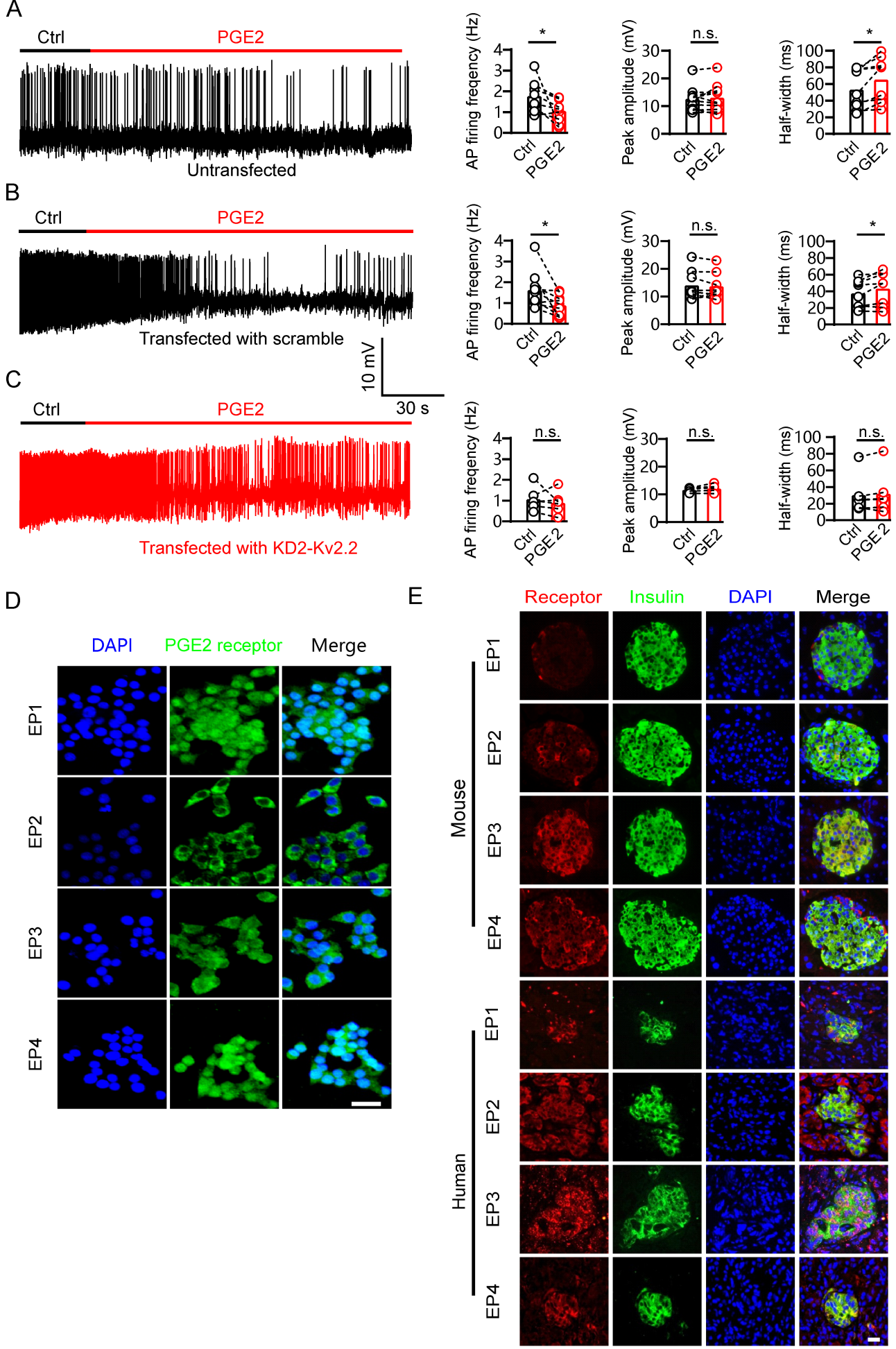
A
Ctrl
PGE2
Untransfected
B
Ctrl
PGE2
Transfected with scramble
10 mV
30 s
C
Ctrl
PGE2
Transfected with KD2-Kv2.2
AP firing freqency (Hz)
Peak amplitude (mV)
Half-width (ms)
Ctrl
PGE2
*
n.s.
D
DAPI
PGE2 receptor
Merge
EP1
EP2
EP3
EP4
E
Receptor
Insulin
DAPI
Merge
Mouse
Human
EP1
EP2
EP3
EP4

Fig. 5

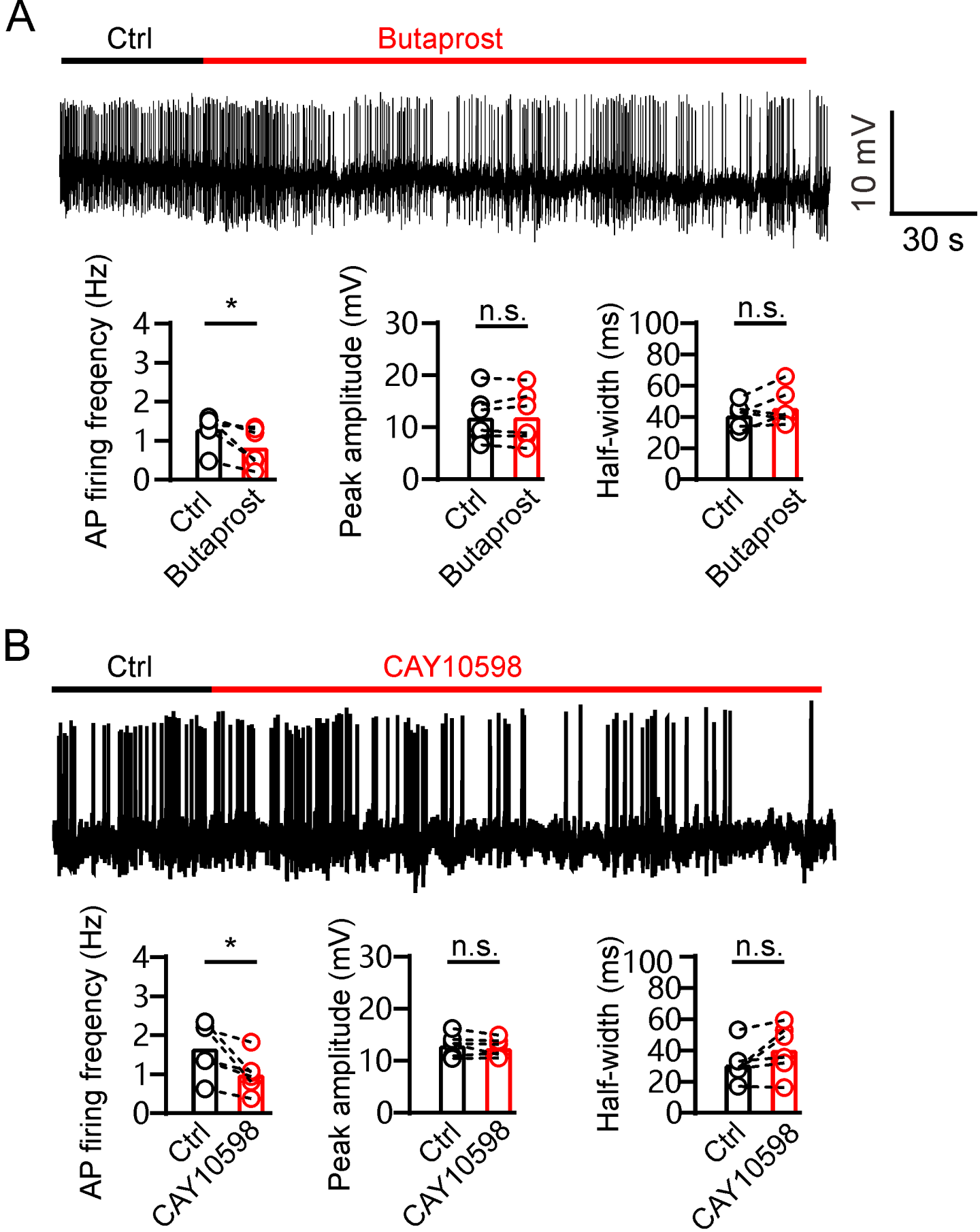
A
Ctrl
Butaprost
10 mV
30 s
AP firing freqency (Hz)
*
Ctrl
Butaprost
Peak amplitude (mV)
n.s.
Half-width (ms)
n.s.
B
Ctrl
CAY10598
AP firing freqency (Hz)
*
Peak amplitude (mV)
n.s.
Half-width (ms)
n.s.

Fig. 6

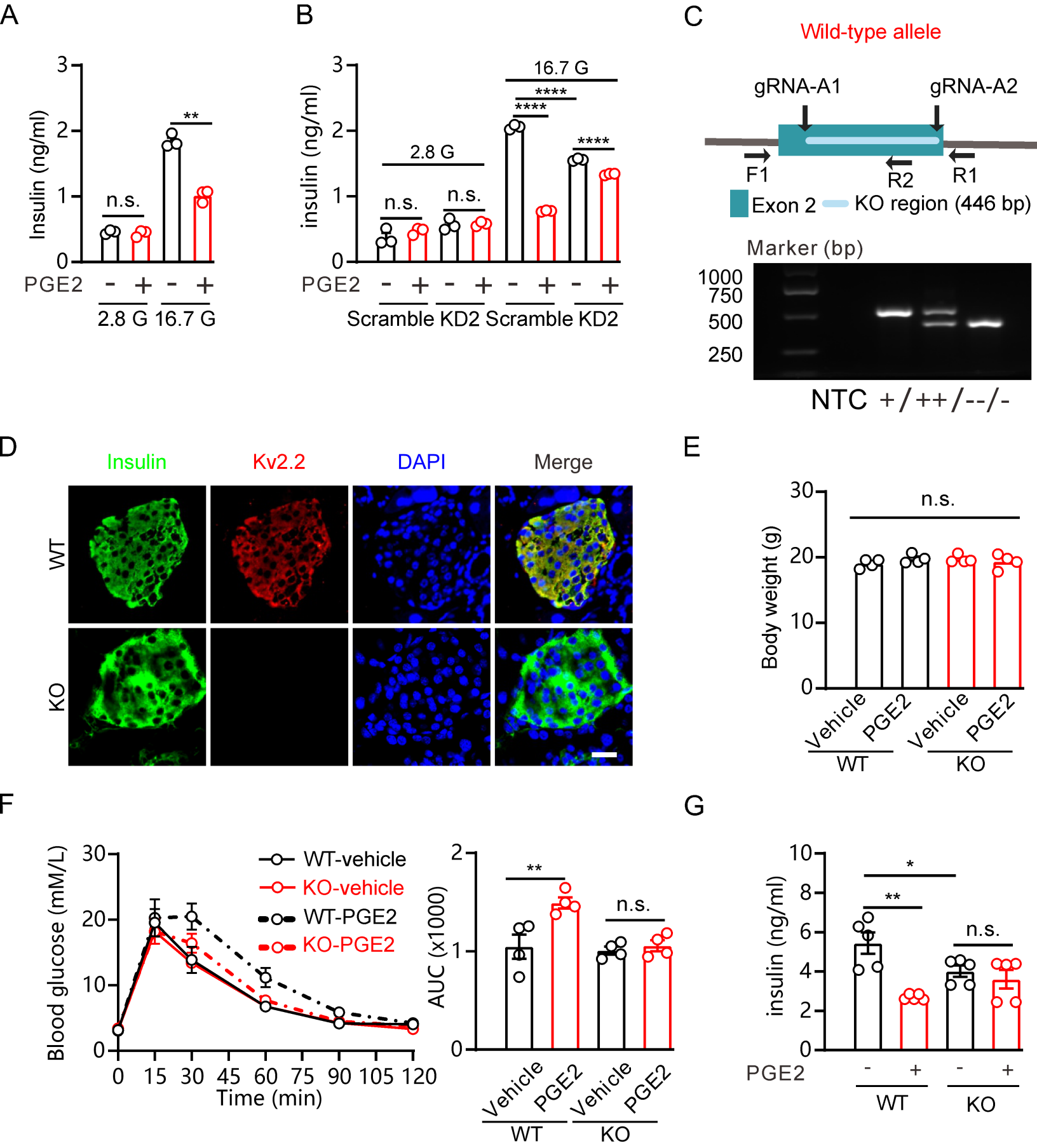
A
Insulin (ng/ml)
n.s.
**
PGE2
2.8 G
16.7 G
B
insulin (ng/ml)
2.8 G
16.7 G
n.s.
n.s.
****
****
****
PGE2
Scramble
KD2
Scramble
KD2
C
Wild-type allele
gRNA-A1
gRNA-A2
F1
R2
R1
Exon 2
KO region (446 bp)
Marker (bp)
1000
750
500
250
NTC
+/+
+/-
-/-
D
Insulin
Kv2.2
DAPI
Merge
WT
KO
E
Body weight (g)
n.s.
Vehicle
PGE2
Vehicle
PGE2
WT
KO
F
Blood glucose (mM/L)
WT-vehicle
KO-vehicle
WT-PGE2
KO-PGE2
Time (min)
AUC (x1000)
**
n.s.
Vehicle
PGE2
Vehicle
PGE2
WT
KO
G
insulin (ng/ml)
*
**
n.s.
PGE2
WT
KO

Fig. 7

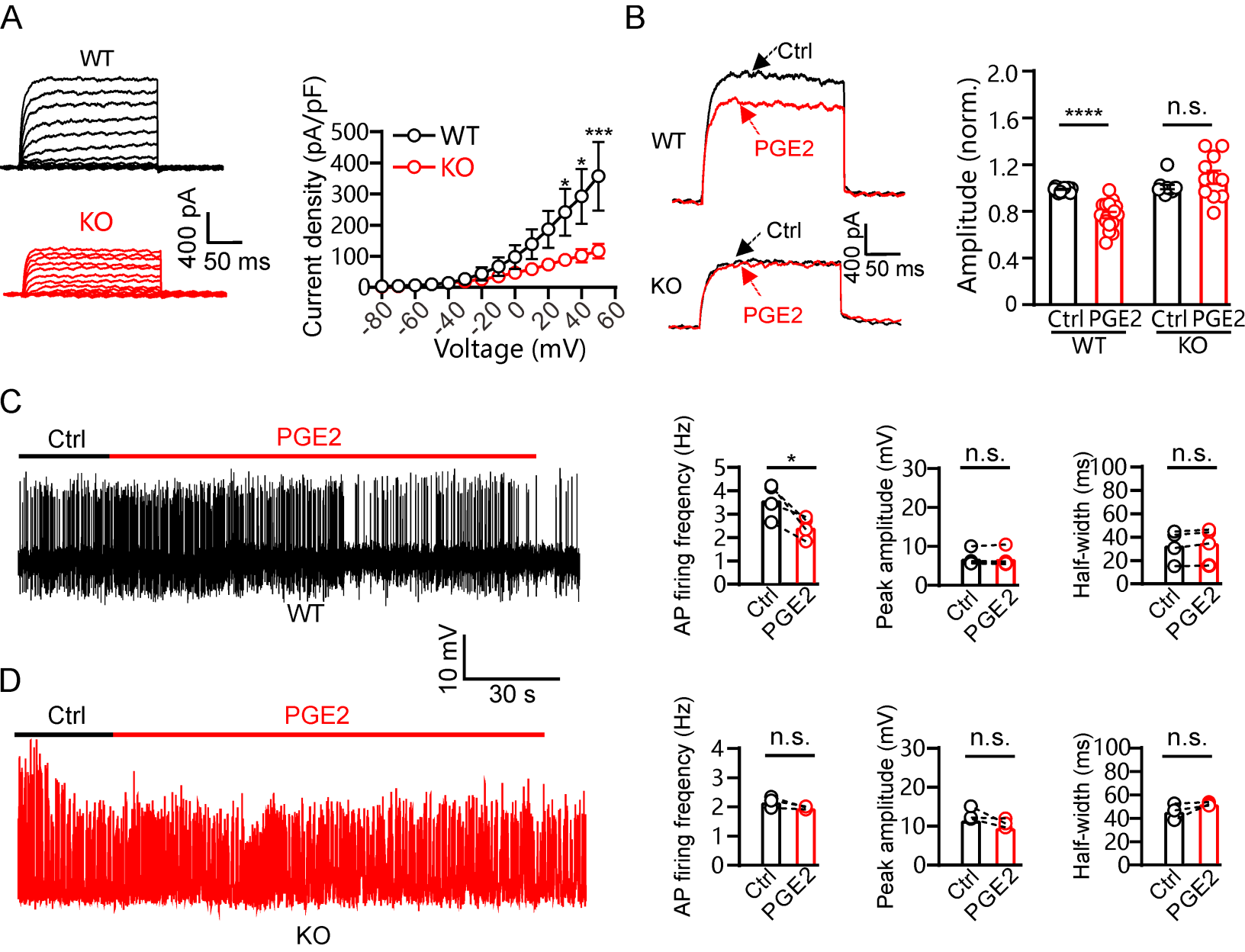
A
WT
KO
400 pA
50 ms
Current density (pA/pF)
500
400
300
200
100
0
WT
KO
*
*
***
-80
-60
-40
-20
0
20
40
60
Voltage (mV)
B
Ctrl
WT
PGE2
Ctrl
KO
PGE2
400 pA
50 ms
Amplitude (norm.)
2.0
1.6
1.2
0.8
0.4
0
****
n.s.
Ctrl PGE2
WT
Ctrl PGE2
KO
C
Ctrl
PGE2
WT
10 mV
30 s
AP firing freqency (Hz)
*
Peak amplitude (mV)
n.s.
Half-width (ms)
n.s.
Ctrl
PGE2
D
Ctrl
PGE2
KO
AP firing freqency (Hz)
n.s.
Peak amplitude (mV)
n.s.
Half-width (ms)
n.s.
Ctrl
PGE2

Fig. 8